

CONTROLLING THREE ATOMIC QUBITS

H. HÄFFNER^{1,2}, M. RIEBE¹, F. SCHMIDT-KALER¹, W. HÄNSEL¹,
C. ROOS¹, M. CHWALLA¹, J. BENHELM¹, T. KÖRBER¹,
G. LANCASTER¹, C. BECHER¹, D.F.V. JAMES³ AND R. BLATT^{1,2}

¹*Institut für Experimentalphysik, Innsbruck, Austria*

²*Institut für Quantenoptik und Quanteninformation, Österreichische Akademie der Wissenschaften, Austria*

³*Theoretical Division T-4, Los Alamos National Laboratory, Los Alamos NM 87545, United States*

We present a series of experiments where up to three ions held in a Paul trap are entangled, a given number of ions is selectively read out while conditional single-quantum-bit (qubit) operations are performed coherently on the remaining ion(s). Using these techniques, we demonstrate also a state transfer of a quantum bit from one ion to another one using two measurements and entanglement between an auxiliary ion and the target ion – also known as teleportation.

1. Introduction

Quantum information processing rests on the ability to control a quantum register¹. In particular this includes initialization, manipulation and read-out of a set of qubits. After initialization, a sequence of quantum gate operations implements the algorithm, which usually generates multi-partite entangled states of the quantum register. Finally, the outcome of the computation is obtained by measuring the state of the individual quantum bits. In addition, for some important algorithms such as quantum error correction^{1,2,3,4,5} and teleportation⁶ a subset of the quantum register is read out selectively and subsequently operations on other qubits are carried out conditioned on the measurement result^a.

This idea of the selective read-out of a quantum register gains some

^aIndeed, such an error-correction scheme been carried out recently in an ion trap by Chiaverini and co-workers⁷ in an ion trap.

additional appeal when carried out on an entangled register, because there the measurement process can be demonstrated in an extraordinary clear way. Producing entangled states is also the key ingredient for quantum information processing, and last but not least, such experiments realize some of the Gedanken experiments which helped significantly to develop quantum mechanics. Creation of entanglement with two or more qubits has already been demonstrated in the references^{8,9,10,11,12,13,14}. However, so far only trapped ions have allowed to create entanglement in a completely deterministic way⁹. Our experiment allows the deterministic generation of 3-qubit entangled states and the selective read-out of an individual qubit followed by local quantum operations conditioned on the read-out. As we will see later, the selective read-out of the quantum register illuminates the measurement process in a very clear way.

The paper is organized as follows: first the deterministic creation of maximally entangled three-qubit states, specifically the Greenberger-Horne-Zeilinger (GHZ) state and the W-state, with a trapped-ion quantum computer is discussed¹⁵. In sections 4 and 5 we show how the qubits can be read out selectively and how GHZ- and W-states are affected by such local measurements. Next we demonstrate in section 6 operations conditioned on the read-out. This enables us to transform tripartite entanglement deterministically into bipartite entanglement with local operations and measurements. It also realizes a quantum eraser along the lines proposed in Ref.¹⁶. Finally, we implement a full deterministic quantum teleportation on demand¹⁷ (see section 7).

2. Experimental setup

All experiments are performed in an elementary ion-trap quantum processor^{18,19}. In order to investigate tripartite entanglement^{20,21,22}, we trap three $^{40}\text{Ca}^+$ ions in a linear Paul trap. Qubits are encoded in a superposition of the $S_{1/2}$ ground state and the metastable $D_{5/2}$ state (lifetime $\tau \simeq 1.16$ s). Each ion-qubit is individually manipulated by a series of laser pulses on the $S \equiv S_{1/2}$ ($m_j=-1/2$) to $D \equiv D_{5/2}$ ($m_j=-1/2$) quadrupole transition near 729 nm employing narrowband laser radiation tightly focused onto individual ions in the string. The entire quantum register is prepared by Doppler cooling, followed by sideband ground state cooling of the center-of-mass vibrational mode ($\omega = 2\pi$ 1.2 MHz). The ions' electronic qubit states are initialised in the S-state by optical pumping.

The operations which modify individual qubits and connect a qubit to

the bus (the center-of mass mode) are performed by applying laser pulses on the carrier ^b or the “blue” sideband ^c of the S→D transition. Qubit rotations can be written as unitary operations in the following way (c.f. ²³): carrier rotations are given by

$$R^C(\theta, \varphi) = \exp \left[i \frac{\theta}{2} (e^{i\varphi} \sigma^+ + e^{-i\varphi} \sigma^-) \right], \quad (1)$$

whereas transitions on the blue sideband are denoted as

$$R^+(\theta, \varphi) = \exp \left[i \frac{\theta}{2} (e^{i\varphi} \sigma^+ a^\dagger + e^{-i\varphi} \sigma^- a) \right]. \quad (2)$$

Here σ^\pm are the atomic raising and lowering operators which act on the electronic quantum state of an ion by inducing transitions from the $|S\rangle$ to $|D\rangle$ state and vice versa (notation: $\sigma^+ = |D\rangle\langle S|$). The operators a and a^\dagger denote the annihilation and creation of a phonon at the trap frequency ω , i.e. they act on the motional quantum state. The parameter θ depends on the strength and the duration of the applied pulse and φ the relative phase between the optical field and the atomic polarization.

Ions are numbered in analogy to binary numbers such that the first ion is the right-most with the least significance. Defining the D -Level as logical 0, we obtain the following ordering of the basis: $|DDD\rangle, |DDS\rangle, |DSD\rangle, \dots$

3. Preparing GHZ- and W-states

Entanglement of three qubits can be divided into two distinct classes²¹: GHZ-states and W-states. Choosing one representative of each class ($|GHZ\rangle \equiv (|SSS\rangle + |DDD\rangle)/\sqrt{2}$ and $|W\rangle \equiv (|DDS\rangle + |DSD\rangle + |SDD\rangle)/\sqrt{3}$) any pure entangled three qubit state can be created by single qubit operations on either $|GHZ\rangle$ or $|W\rangle$. We synthesize GHZ-states using a sequence of 10 laser pulses (Tab. 1) and W-states with a sequence of five laser pulses (see Tab. 2). These pulse sequences generate three-ion entangled states within less than 1 ms.

Full information on the three-ion entangled states is obtained by state tomography. For this the entangled states are subjected to 27 different sets of single qubit operations before the read-out employing a CCD camera. From this data all 64 entries of the density matrix are extracted with the methods described in ^{24,26}. In total 5000 experiments –corresponding to

^b $|S, n\rangle \rightarrow |D, n\rangle$ transition, i.e. no change of vibrational quantum number n , laser on resonance

^c $|S, n\rangle \rightarrow |D, n+1\rangle$, laser detuned by $+\omega$

Table 1. Pulse sequence to create the GHZ-state ($|GHZ\rangle \equiv (|DDD\rangle + i|SSS\rangle)/\sqrt{2}$). For the definitions of $R_i^{C,+}(\theta, \varphi)$ see Eq. 1 and 2. First we apply a so-called beamsplitter pulse, creating a correlation between ion #1 and the bus mode (the phonon qubit). Ion #2 is flipped conditional on the phonon qubit with a CNOT-operation consisting of a phase gate³⁹ enclosed in two Hadamard-like operations. Finally the phonon qubit is mapped onto ion #3.

ion #1 (beamsplitter)	$R^+(\pi/2, 0)$	$R^C(\pi, \pi/2)$		
ion #2 (Hadamard)	$R^C(\pi/2, 0)$			
ion #2 (Phase gate)	$R^+(\pi, \pi/2)$	$R^+(\pi/\sqrt{2}, 0)$	$R^+(\pi, \pi/2)$	$R^+(\pi/\sqrt{2}, 0)$
ion #2 (Hadamard)	$R^C(\pi/2, \pi)$			
ion #3 (map)	$R^C(\pi, 0)$	$R^+(\pi, 0)$		

Table 2. Pulse sequence to create the W-state. First we apply an asymmetric beamsplitter pulse on ion #2 exiting the phonon mode with a probability of one-third. If the the phonon mode is excited, the second beamsplitter sequence removes the phonon with a probability of 0.5 and maps it onto ion #3. Finally, the last pulse maps the remaining phonon population onto ion #1 and we obtain $(|DDS\rangle + |DSD\rangle + |SDD\rangle)/\sqrt{3}$.

ion #2 (beamsplitter)	$R^+(2 \arccos(1/\sqrt{3}), 0)$	
ion #3 (beamsplitter)	$R^C(\pi, \pi)$	$R^+(\pi/2, \pi)$
ion #1 (map)	$R^C(\pi, 0)$	$R^+(\pi, \pi)$

200 s of measurement time– are sufficient to achieve an uncertainty of less than 2% for all density matrix elements.

In Fig. 1 and 2 we show the experimental results for the density matrix elements of the GHZ and W-states, $\rho_{|GHZ\rangle}$ and $\rho_{|W\rangle}$. The off-diagonal elements are observed with nearly equal height as the corresponding diagonal elements and with the correct phases. Fidelities of 76%??? for $\rho_{|GHZ\rangle}$ and 83%??? for $\rho_{|W\rangle}$ are obtained. The fidelity is defined as $|\langle \Psi_{\text{ideal}} | \rho_{\text{exp}} | \Psi_{\text{ideal}} \rangle|^2$ with Ψ_{ideal} denoting the ideal quantum state and ρ_{exp} the experimentally determined density matrix.

All sources of imperfections have been investigated independently¹⁹ and the measured fidelities are consistent with the known error budget. Note that for the W-state, coherence times greater than 200 ms were measured (exceeding the synthesis time by almost three orders of magnitude), while for the GHZ-state only ~ 1 ms was found. This is due to the W-states being a superposition of three states with the same energy. Thus, the W-states are not sensitive to the overall energy scale of the system and laser frequency noise does not lead to dephasing. This is in strong contrast to the GHZ-state in Fig. 2 which is maximally sensitive to such perturbations. Similar behaviour has been observed previously with Bell-states^{25,26}.

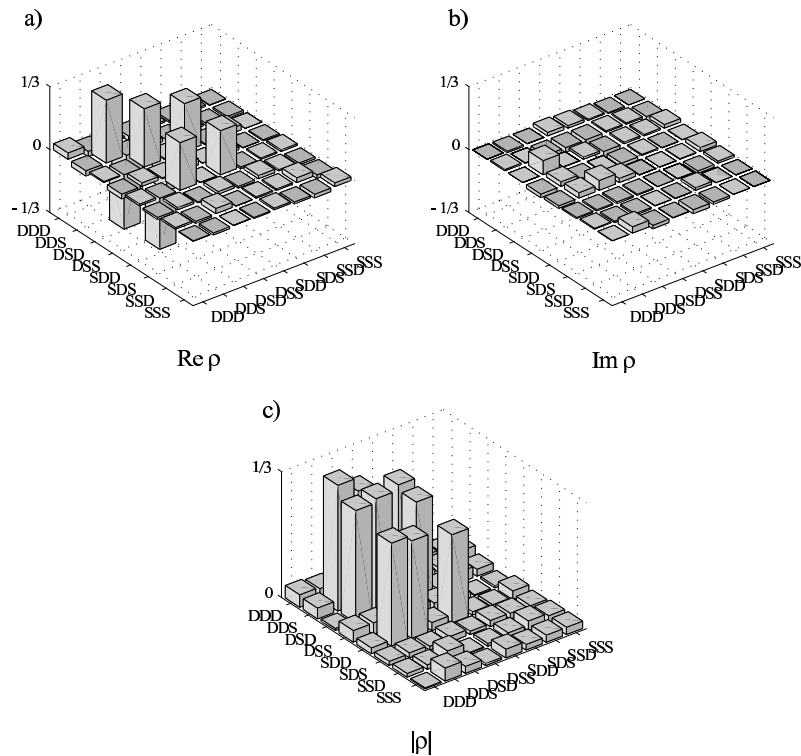


Figure 1. Real part (a), imaginary part (b) and absolute values (c) of the density matrix elements of the experimentally obtained W quantum state. The off-diagonal elements are of equal height as the diagonal elements and indicate the coherence between the different logical eigenstates $\{D, S\}$. The fidelity is calculated to be 83 %???

4. Projection of the quantum states by measurement

Having tripartite entangled states available as a resource, we make use of individual ion addressing to project one of the three ions' quantum state to an energy eigenstate while preserving the coherence of the other two. Qubits are protected from being measured by transferring their quantum information into superpositions of levels which are not affected by the detection, that is a light scattering process on the $S_{1/2} \rightarrow P_{1/2}$ -transition. In Ca^+ , an additional Zeeman level $D' \equiv D_{5/2}$ ($m_j = -5/2$) can be employed for this purpose. Thus, after the state synthesis, we apply two π pulses on the $S \rightarrow D'$ transition of ion #1 and #2, moving any S population of these ions into their respective D' level. The D and D' levels do not couple to the detection light at 397 nm (Fig. 3).

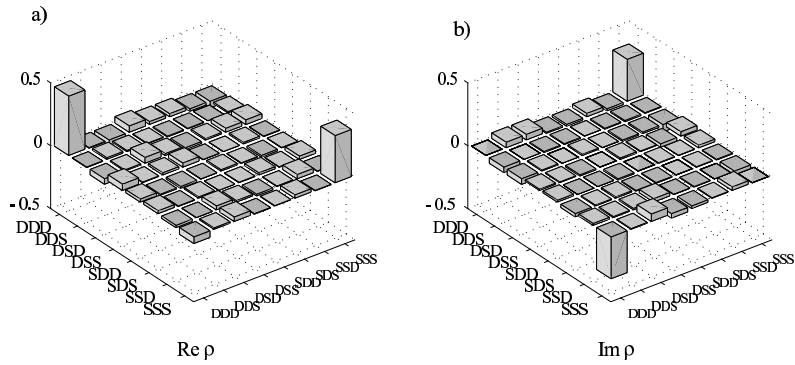


Figure 2. Real (a) and imaginary (b) elements of a GHZ-states density matrix. The off-diagonal elements for SSS and DDD indicate the quantum correlation (coherences). The fidelity was calculated to be 76 %.

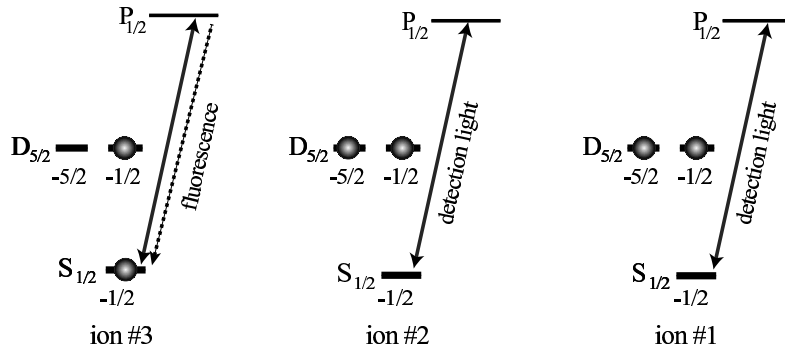


Figure 3. Partial level scheme of the three Ca-ions. Only ion #3 is read out. Ion #1 and #2's quantum information is protected in the Zeeman manifold of the $D_{5/2}$ -level, namely the $m_J = -1/2$ and $m_J = -5/2$ levels. Note that we have labelled the ions in analogy to a binary number representation from right to left.

Therefore, ion #3 can be read out using electron shelving¹⁹. After the selective readout a second set of π -pulses on the D' to S transition transfers the quantum information back into the original computational subspace {D, S}.

For a demonstration of this method, GHZ- and W-states are generated and the qubits #1 and #2 are mapped onto the {D, D'} subspace. Then, the state of ion #3 is projected onto S or D by scattering photons for a few microseconds on the S-P transition. In a first series of experiments, we did not distinguish whether ion #3 was projected into S or D. After remapping

qubits #1 and #2 to the original subspace $\{S, D\}$, the tomography procedure is applied to obtain the full density matrix of the resulting three-ion state. As shown in Fig. 4c, the GHZ-state is completely destroyed, i.e.

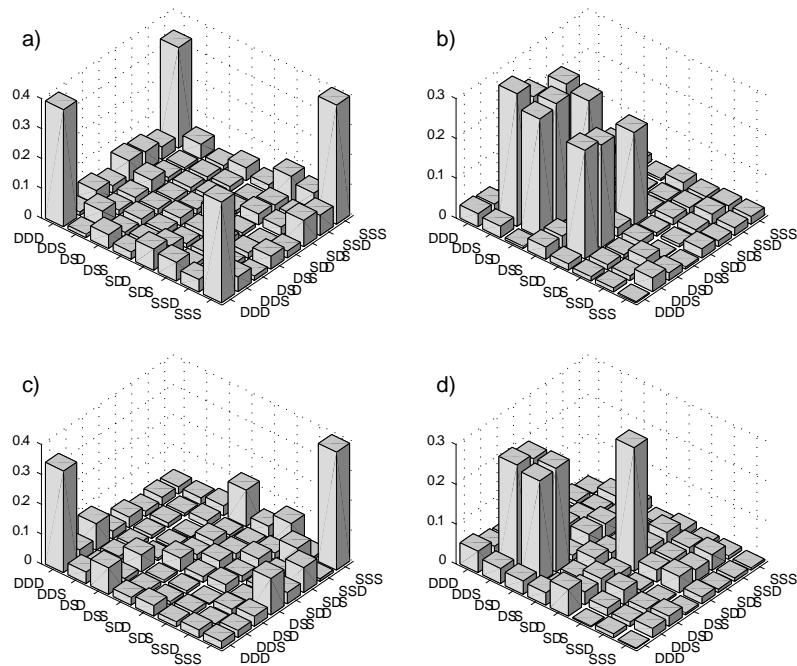


Figure 4. Absolute values of density matrices after measuring ion #3. (a) shows the density matrix of a GHZ-state before measuring and (c) after ion #3 is measured. The same for a W-state ((b) and (d)).

it is projected into a mixture of $|SSS\rangle$ and $|DDD\rangle$. In contrast, for the W-state, the quantum register remains partially entangled as coherences between ion #1 and #2 persist (Fig. 4c). Note that related experiments have been carried out with mixed states in NMR¹⁴ and with photons¹².

5. Selective read-out of a quantum register

In a second series of experiments with W-states, we deliberately determine the third ion's quantum state prior to tomography: The ion string is now illuminated for $500 \mu\text{s}$ with light at 397 nm and its fluorescence is collected with a photomultiplier tube (Fig. 5a). Then, the state of ion #3 is known and subsequently we apply the tomographic procedure to ion #1 and #2

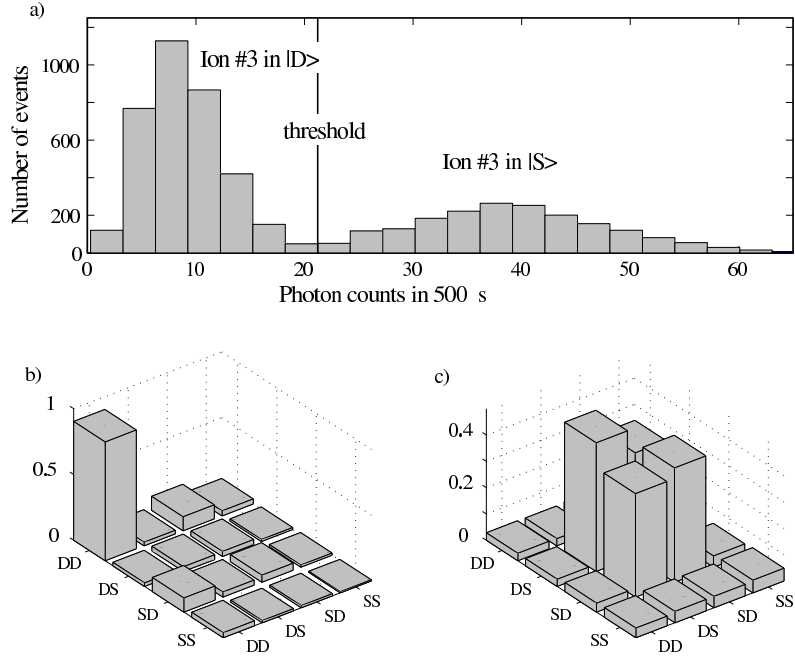


Figure 5. (a) Histogram of photon counts within 500 s for ion #3 and threshold setting. (b) and (c) Density matrix of ion #1 and #2 conditioned upon the previously determined quantum state of ion #3. The absolute values of the reduced density matrix are plotted for ion #3 measured in the S state (b) and ion #3 measured in the D state (c). Off-diagonal elements in (b) show the remaining coherences.

after remapping them to their $\{S, D\}$ subspace. Depending on the state of ion #3, we observe the two density matrices presented in Fig. 5B and 5C. Whenever ion #3 was measured in D, ion #1 and #2 were found in a Bell state $(|SD\rangle + |DS\rangle)/\sqrt{2}$, with a fidelity of 82%. If the third qubit was observed in S, the resulting state is $|DD\rangle$ with fidelity of 90%. This is a characteristic signature of $W \equiv (|DDS\rangle + |DSD\rangle + |SDD\rangle)/\sqrt{3}$: In $1/3$ of the cases, the measurement projects qubit #3 into the S state, and consequently the other two qubits are projected into D. With a probability of $2/3$ however, the measurement shows qubit #3 in D, and the remaining quantum register is found in a Bell state²¹. Experimentally, we observe the third ion in D in 65 (2)% of the cases.

6. Conditioned single qubit operations

In section 4 we found that measuring a single qubit destroys the quantum nature of a GHZ-state completely. However, if prior to this the qubit is rotated into a different basis, the quantum nature of the GHZ-state can be partially preserved. Moreover, we can deterministically transform tripartite entanglement into bipartite entanglement using only local measurements and one-qubit operations. To demonstrate this, we first generate the GHZ-state $(|DSD\rangle + |SDS\rangle)/\sqrt{2}$. In a second step, we apply a $\pi/2$ pulse to ion #3, with phase $3\pi/2$, rotating a state $|S\rangle$ to $(|S\rangle - |D\rangle)/\sqrt{2}$ and $|D\rangle$ to $(|S\rangle + |D\rangle)/\sqrt{2}$, respectively. The resulting state of the three ions is $|D\rangle(|SD\rangle - |DS\rangle) + |S\rangle(|SD\rangle + |DS\rangle)/2$. A measurement of the third ion, resulting in $|D\rangle$ or $|S\rangle$, projects qubits #1 and #2 onto the state $(|SD\rangle - |DS\rangle)/\sqrt{2}$ or the state $(|SD\rangle + |DS\rangle)/\sqrt{2}$, respectively. The corresponding density matrix is plotted in Fig. 6a. With the information of the state of

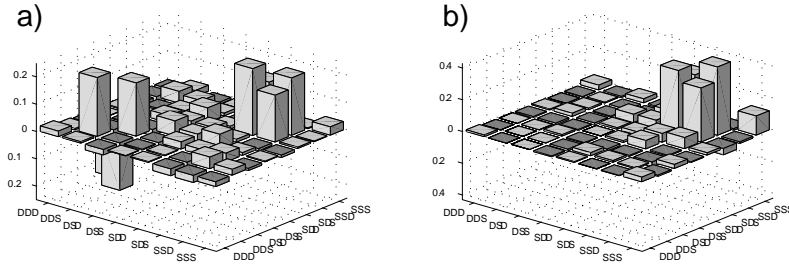


Figure 6. (a) Real part of the density matrix elements of the system after ion #1 of the GHZ-state $(|DSD\rangle + |SDS\rangle)/\sqrt{2}$ has been measured in a rotated basis. (b) Transformation of the GHZ-state $(|DSD\rangle + |SDS\rangle)/\sqrt{2}$ into the bipartite entangled state $|S\rangle(|SD\rangle + |DS\rangle)/\sqrt{2}$ by conditional local operations. Note the different vertical scaling of (a) and (b).

ion #3 available, we can now transform this mixed state into the pure state $|S\rangle(|SD\rangle + |DS\rangle)/\sqrt{2}$ by local operations only. Provided that ion #3 is found in $|D\rangle$, we perform a so-called Z-gate $(R^C(\pi, \pi/2)R^C(\pi, 0))$ on ion #2 to obtain $|D\rangle(|SD\rangle + |DS\rangle)/\sqrt{2}$. In addition, we flip the state of ion #3 to reset it to $|S\rangle$. Figure 6b shows that the bipartite entangled state $|S\rangle(|SD\rangle + |DS\rangle)/\sqrt{2}$ is produced with fidelity of 75%. This procedure can also be regarded as an implementation of a three-spin quantum eraser as proposed in¹⁶.

Our results show that selectively reading out a qubit of a quantum register indeed leaves all other qubits in the register untouched. In partic-

ular that means that for certain states entanglement can be preserved in the remaining part of the quantum register. In addition, even after such a measurement has taken place, single qubit rotations can be performed with high fidelity. Such techniques mark a first step towards the one-way quantum computer²⁷. The implementation of unitary transformations conditioned on measurement results has great impact as it provides a way to implement active quantum-error-correction algorithms. In addition, we will show in the next sections that it allows for the realization of deterministic quantum teleportation.

7. Teleportation

Quantum teleportation exploits some of the most fascinating features of quantum mechanics, in particular *entanglement*, shedding new light on the essence of quantum information. It is possible to transfer the quantum information contained in a two-level system –a qubit– by communicating two classical bits and using entanglement. Thus quantum information can be broken down in a purely classical part and a quantum part.

Furthermore, teleportation is not merely a simple swapping of quantum states: it does not need a quantum channel to be open at the time the transfer is carried out. Instead it uses the non-local properties of quantum mechanics (entanglement), established by a quantum channel *prior to the generation of the state to be teleported*. Once that link has been established, an unknown state can be transferred at any later time using classical communication only. This is quite surprising since the quantum part of the transfer seems to have happened before the state to be transferred exists. In addition to the motivation to demonstrate and to understand quantum physics, teleportation might also have considerable impact on a future quantum computer as it facilitates the scalability of many quantum computer designs²⁸.

Teleportation was already demonstrated with photonic qubits^{29,30,11,31,32}. However, these experiments did not include complete two-photon Bell state measurements. In addition, successful teleportation events were established by selecting the data after completion of the experiment, searching for the subset of experiments in which the outcome of the measurement and a preset reconstruction operation were matched: i.e. teleportation was performed post-selectively. In contrast to this the experiment by Furusawa et al.³³ demonstrated unconditional teleportation of continuous variables. Similarly Nielsen et al.³⁴ implemented a determinis-

tic teleportation algorithm with highly mixed states in a liquid-state NMR set-up.

Recently two groups realized quantum teleportation of atomic qubits. The Boulder group³⁵ teleported the quantum information contained in one Beryllium-ion to another one, while the Innsbruck group¹⁷ used Calcium ions for the same purpose. Both groups trap their ions in Paul trap, however, pursue a different approaches: in Boulder the qubits are encoded in the hyperfine structure of the ions, while in Innsbruck the qubit states are stored in superpositions of a ground and metastable electronic state. Furthermore the Boulder group uses segmented traps to perform the required selective read-out of the quantum register, whereas in Innsbruck tightly focused laser beams together with selective excitation of the Zeeman levels are employed for this purpose. Finally the Boulder group chose to work with a geometric phase gate³⁶, while the Innsbruck group uses composite pulses to realize the phase gate¹⁸. Despite these different approaches both experiments yield similar results. This demonstrates that ions traps are versatile devices for coherent state manipulation and quantum information processing.

The teleportation of a state from a source qubit to a target qubit requires three qubits: the sender's source qubit and an ancillary qubit that is maximally entangled with the receiver's target qubit providing the strong quantum correlation. In our experiments, each qubit is represented by a superposition of the $S_{1/2}(m_j = -1/2) \equiv |S\rangle$ ground state and the $D_{5/2}(m_j = -1/2) \equiv |D\rangle$ metastable state of a $^{40}\text{Ca}^+$ ion. All three ions are stored together in a linear Paul trap and arrange themselves as a string with an inter-ion distance of $5 \mu\text{m}$. Each qubit can be individually manipulated by a series of laser pulses on the $|S\rangle \rightarrow |D\rangle$ quadrupole transition near 729 nm employing narrow-band laser radiation tightly focused onto individual ions in the string. The qubits are initialized in $|S\rangle$ by optical pumping. The ion string's center-of-mass vibrational mode ($\omega = 2\pi \times 1.2 \text{ MHz}$) is cooled to the ground state as required for controlled interaction between the ions according to the original proposal by Cirac and Zoller³⁷. For further experimental details see ref. ¹⁹.

The quantum teleportation circuit is displayed in Fig. 7. The circuit is formally equivalent to the one proposed by Bennett *et al.*⁶, but adapted to the ion-based quantum processor. It can be broken up in the following tasks:

- (1) **Creation of Bell states**

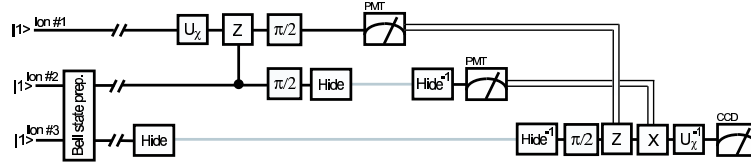


Figure 7. The teleportation algorithm's quantum circuit. Double lines represent flow of classical information, whereas single lines flow of quantum information. The shaded lines indicate when a qubit is protected from detection light via so-called hiding-pulses. First ions #2 and #3 are entangled, creating the quantum link between the source region (ions #1 and #2) and the target ion (ion #3). Then after some waiting time the state to be teleported (on ion #1) is prepared via the unitary operation U_χ . A controlled Z -gate together with detection via a photomultiplier tube (PMT) realizes the Bell state measurement. After the reconstruction pulses the success of the teleportation is tested by applying the inverse preparation procedure before measuring the target ion on an intensified CCD-camera (Charged Coupled Device).

A pulse sequence of three laser pulses (cf. Tab. 3) produces the Bell-state $(|DS\rangle + |SD\rangle)/\sqrt{2}$. Tomography^{38,26} of this state shows a fidelity of up to 96% for the entangling operation. Similarly to the W -states above this Bell state consists of a superpositions of states with the same energy. Indeed, we observe that the lifetime of this Bell state approaches the fundamental limit given by the spontaneous decay rate of the metastable $D_{5/2}$ -level of 1.2 s^{26} . Now, after the quantum link between the source and the target region is established, we prepare a test state χ via a single qubit operation U_χ on the source ion.

(2) Rotation into the Bell-basis

The Bell-state measurement is accomplished by rotating the basis of the source and the ancilla ion into the Bell basis before the actual read-out of the qubits. This rotation is implemented with a controlled- Z (phase) gate and appropriate single qubit operations. The experimental implementation of the controlled- Z -gate is described in ref. ¹⁸. To illustrate the rotation into the Bell-basis more easily, we will use in the following a zero-controlled-not (0-CNOT) gate as a substitute for the controlled Z -gate: suppose one has the Bell state $(|DS\rangle + |SD\rangle)/\sqrt{2}$ (note that we use the convention $|D\rangle \equiv |0\rangle$ and $|S\rangle \equiv |1\rangle$), then application of a 0-CNOT followed by

a $\pi/2$ -Carrier-Pulse on the control bit (the leftmost bit) yields:

$$\begin{aligned} (|DS\rangle + |SD\rangle)/\sqrt{2} &\xrightarrow{0-CNOT} (|DD\rangle + |SD\rangle)/\sqrt{2} & (3) \\ &= (|D\rangle + |S\rangle)|D\rangle/\sqrt{2} \xrightarrow{R_C^C(\pi/2,0)} |SD\rangle & (4) \end{aligned}$$

The pulse $R_C^C(\pi/2, 0)$ denotes a single qubit rotation onto the control bit. Now we have mapped the Bell state $|DS\rangle + |SD\rangle$ to $|SD\rangle$. Similarly all other Bell states are mapped onto orthogonal logical eigenstates. Therefore a measurement in the logical eigenbasis yields now a precise knowledge of the original Bell state.

(3) **Selective read-out of the quantum register and conditional quantum gates**

The measurement process must preserve the coherence of the target qubit, ion #3. Thus, the state of ion #3 is hidden by transferring it to a superposition of levels which are not affected by the detection light. We employ an additional Zeeman level of the $D_{5/2}$ manifold for this purpose. Applying now laser light at 397 nm for 250 μ s to the ion crystal, only the ion in question can fluoresce, and that only if it is the $S_{1/2}$ -state¹⁵. This hiding technique is also used to sequentially read out ion #1 and ion #2 with a photomultiplier tube (see Fig. 3). Instead of using a CCD-camera (which can easily distinguish between different ions), we prefer to take advantage of the fast electronic read-out capabilities of a photo-multiplier tube. This ensures a reaction on the measurement result within the single qubit coherence time. A digital electronic circuit counts the number of detected photons and compares it to the threshold (less than 6 detected photons indicate that the ion is in the $D_{5/2}$ level).

Conditioned on the measurement result, we apply single qubit rotations on the target ion¹⁵. This is implemented by using a classical AND-gate between the output of the electronic circuit which has stored the measurement result and the output of a Digital board on which the reconstruction pulses are programmed. Thus, we apply the appropriate unitary qubit rotation, $-i\sigma_y$, $-i\sigma_z$, $i\sigma_x$, or 1 (with Pauli operators σ_k) to reconstruct the state in the target ion #3, obtaining χ on ion #3. Note that $-i\sigma_z$ is realized by applying $\sigma_x\sigma_y$. This has the advantage that we can apply σ_x if ion #1 is measured to be in $|D\rangle$ and σ_z if ion #2 is measured to be in $|D\rangle$ and can keep so the electronic logic quite simple.

The whole pulse sequence is displayed in Tab. 3. In contrast to Fig.7, here

also spin echo pulses are included. The conditioned pulses #31,32,33 are applied only if less than 6 photon detection events were recorded during the respective detection time of $250 \mu\text{s}$. The phase ϕ for the pulses is fixed during all experiments. It is used to compensate for the 50 Hz related magnetic field fluctuations during the execution of the teleportation algorithm.

To obtain directly the fidelity of the teleportation, we perform on ion #3 the operation U_χ^{-1} , which is the inverse of the unitary operation used to create the input state $|\chi\rangle$ from state $|S\rangle$ (see pulses #9 and #34 in Tab. 3). The teleportation is successful if and only if ion #3 is always found in $|S\rangle$. The teleportation fidelity, given by the overlap $F = \langle S|U_\chi^{-1}\rho_{\text{exp}}U_\chi|S\rangle$, is plotted in Fig. 8 for all four test states $\{|S\rangle, |D\rangle, |S+D\rangle, |S+iD\rangle\}$. The obtained fidelities range from 73% to 76%. Teleportation based on

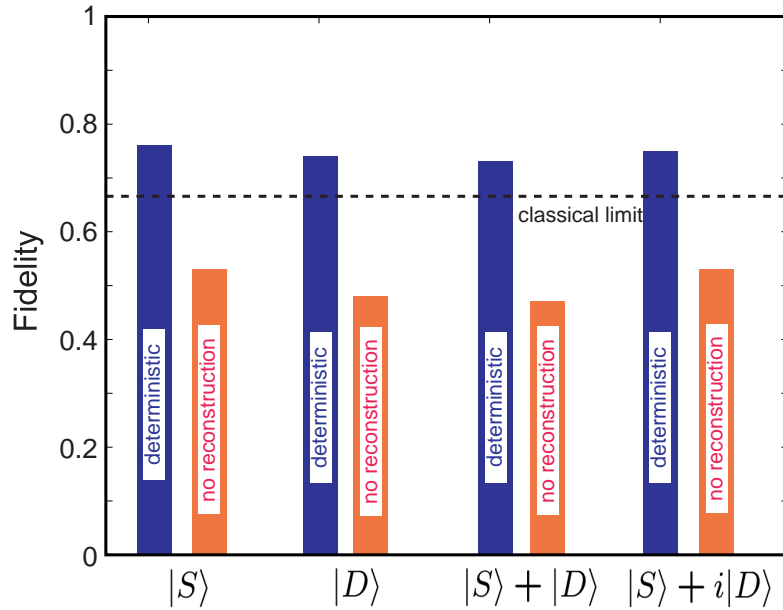


Figure 8. Result of the teleportation: The four test states are teleported with fidelities of 76%, 74%, 73%, and 75%, respectively (grey bars). For each input state 300 single teleportation experiments were performed. The error of each entry, estimated from quantum projection noise, is 2.5%. The red bars show the results if the reconstruction operations are omitted, yielding an average fidelity of 49.6%. The optimum teleportation obtainable by purely classical means and no assumptions about the initial states reaches a fidelity of 66.7% (dashed line).

a completely classical resource instead of a quantum entangled resource

Table 3. To implement the teleportation, we use pulses on carrier transitions $R_i^C(\theta, \varphi)$ and $R_i^H(\theta, \varphi)$ (no change of the motional state of the ion crystal) and, additionally, on the blue sideband $R_i^+(\theta, \varphi)$ (change of the motional state) on ion i . The index C denotes carrier transitions between the two logical eigenstates, while the index H labels transitions from the $S_{1/2}(m_J = -1/2)$ to the $D_{5/2}(m_J = -5/2)$ -level. For the definitions of $R_i^{C,H,+}(\theta, \varphi)$ see the refs. ³⁹ and ¹⁸.

	Action	Comment
	1 Light at 397 nm	Doppler preparation
	2 Light at 729 nm	Sideband cooling
	3 Light at 397 nm	Optical pumping
Entangle	4 $R_3^+(\pi/2, 3\pi/2)$	Entangle ion #3 with motional qubit
	5 $R_2^C(\pi, 3\pi/2)$	Prepare ion #2 for entanglement
	6 $R_2^+(\pi, \pi/2)$	Entangle ion #2 with ion #3
	7 Wait for $1\mu\text{s} - 10\,000\ \mu\text{s}$	Stand-by for teleportation
	8 $R_3^H(\pi, 0)$	Hide target ion
	9 $R_1^C(\vartheta_\chi, \varphi_\chi)$	Prepare source ion #1 in state χ
Rotate into Bell-basis	10 $R_2^+(\pi, 3\pi/2)$	Get motional qubit from ion #2
	11 $R_1^+(\pi/\sqrt{2}, \pi/2)$	Composite pulse for phasegate
	12 $R_1^+(\pi, 0)$	Composite pulse for phasegate
	13 $R_1^+(\pi/\sqrt{2}, \pi/2)$	Composite pulse for phasegate
	14 $R_1^+(\pi, 0)$	Composite pulse for phasegate
	15 $R_1^C(\pi, \pi/2)$	Spin echo on ion #1
	16 $R_3^H(\pi, \pi)$	Unhide ion #3 for spin echo
	17 $R_3^C(\pi, \pi/2)$	Spin echo on ion #3
	18 $R_3^H(\pi, 0)$	Hide ion #3 again
	19 $R_1^+(\pi, \pi/2)$	Write motional qubit back to ion #2
	20 $R_1^C(\pi/2, 3\pi/2)$	Part of rotation into Bell-basis
21 $R_2^C(\pi/2, \pi/2)$	Finalize rotation into Bell basis	
Read-out	22 $R_2^H(\pi, 0)$	Hide ion #2
	23 PMDetection for $250\ \mu\text{s}$	Read out ion #1 with photomultiplier
	24 $R_1^H(\pi, 0)$	Hide ion #1
	25 $R_2^H(\pi, \pi)$	Unhide ion #2
	26 PMDetection for $250\ \mu\text{s}$	Read out ion #2 with photomultiplier
	27 $R_2^H(\pi, 0)$	Hide ion #2
	28 Wait $300\ \mu\text{s}$	Let system rephase; part of spin echo
	29 $R_3^H(\pi, \pi)$	Unhide ion #3
	30 $R_3^C(\pi/2, 3\pi/2 + \phi)$	Change basis
Recon- struction	31 $R_3^C(\pi, \phi)$	$\left. \begin{array}{l} i\sigma_x \\ -i\sigma_y \end{array} \right\} = -i\sigma_z$ conditioned on PMDetection #1
	32 $R_3^C(\pi, \pi/2 + \phi)$	
	33 $R_3^C(\pi, \phi)$	$i\sigma_x$ conditioned on PMDetection #2
	34 $R_3^C(\vartheta_\chi, \varphi_\chi + \pi + \phi)$	Inverse of preparation of χ with offset ϕ
	35 Light at 397 nm	Read out ion #3 with camera

yields a maximal possible fidelity of 66.7% ⁴¹ (dashed line in Fig. 8). Note that this classical boundary holds only if no assumptions on the states to

be teleported are made. If one restricts oneself to only the four test states, strategies exist which use no entanglement and yield fidelities of 78%⁴⁰. However, each of these strategies must be designed for a specific test state ensemble to work properly. Note also that, in order to rule out hidden variable theories, a fidelity in excess of 0.87 is required⁴².

For comparison, we also show data where the reconstruction pulses were not applied. Without the classical information obtained from the Bell state measurement, the receiver's state is maximally mixed, i.e. there is no information available on the source state. Also, the measurement outcome of ions #1 and #2 does not contain any information about the initial state. Indeed we find each possible result with an equal probability of 0.25 ± 0.036 , independent of the test input states. Note that only with both the receiver's qubit and the result of the Bell measurement, the initial state can be retrieved.

We emphasize that the conditional, deterministic reconstruction step, in combination with the complete Bell state analysis, is one of the crucial improvements with respect to former experimental realizations of quantum teleportation. Furthermore, after the teleportation procedure the state χ is always available and may be used for further experiments.

To emphasize the role of the shared entangled pair as a resource, we store the Bell state for some time and then use it only later (after up to 20 ms) for teleportation. For waiting times of up to 20 ms (exceeding the time we require for the teleportation by a factor of 10) we observe no decrease in the fidelity. For longer waiting times, we expect the measured heating of the ion crystal of smaller than 1 phonon/100 ms to reduce the fidelity significantly. This is because for a successful rotation into the Bell-basis we require the phonon number in center-of-mass mode of the ion string to be in the ground state.

The obtainable fidelity is limited mainly by dephasing mechanisms. The most obvious one is frequency fluctuations of the laser driving the qubit transition, and magnetic field fluctuations. Since these fluctuations are slow compared to the execution time of 2 ms, they can be cancelled to some degree with spin echo techniques⁴³. However, during the algorithm we have to use different pairs of states to encode the quantum information, one of which being only sensitive to magnetic field fluctuations while the other one being sensitive to both laser and magnetic field fluctuations. To overcome these complications, two spin echo pulses are introduced (see Tab. 3). Their optimal position in time was determined with numerical simulations. From measurements we estimate that the remaining high frequency noise reduces

the fidelity by about 5%. Another source of fidelity loss is an imperfect AC-Stark shift compensation. AC-Stark compensation is needed to get rid of the phase shifts introduced by the laser driving the weak sideband transition due to the presence of the strong carrier transitions⁴⁴. Recent measurements suggest that an imperfect compensation as introduced by the incorrect determination of the sideband frequency by only 100 Hz lead to a loss of teleportation fidelity on the order of 5%.

Imperfect state detection as introduced by a sub-optimal choice for the threshold (6 instead of 3 counts) was analyzed later to contribute on the order of 3% to the fidelity loss. However, the biggest contribution to the read-out error stems from an incorrect setting of the hiding pulse frequency and strength. It reduced the fidelity by 7%.

Addressing errors on the order of 3–4% were estimated via numerical simulations to reduce the fidelity by about 6%. The addressing errors were measured by comparing the Rabi flopping frequency between neighboring ions and corresponds to a ratio of 10^{-3} in intensity between the addressed ion and the other ones.

Treating these estimated error sources independently (multiplying the success probabilities) yields an expected fidelity of 77% in good agreement with the experimental findings.

In conclusion, we described an experiment demonstrating teleportation of atomic states. The experimental procedures might be applied in future quantum information processing networks: with long lived entangled states as a resource, quantum teleportation can be used for the distribution of quantum information between different nodes of the network.

We gratefully acknowledge support by the European Commission (QUEST and QGATES networks), by the ARO, by the Austrian Science Fund (FWF). H.H. acknowledges funding by the Marie-Curie-program of the European Union. T.K. acknowledges funding by the Lise-Meitner program of the FWF. We are also grateful for discussions with A. Steinberg and H. Briegel.

References

1. M. A. Nielsen, I. L. Chuang, *Quantum Computation and Quantum Information* (Cambridge Univ. Press, Cambridge, 2000).
2. P. W. Shor, *Phys. Rev. A* **52**, R2493 (1995).
3. A. M. Steane, *Phys. Rev. Lett.* **77**, 793 (1996).
4. C. H. Bennett, D. P. DiVincenzo, J.A. Smolin, W. K. Wootters, *Phys. Rev. A* **54**, 3824 (1996).

5. A. M. Steane, *Nature* **399**, 124 (1999).
6. Bennett, C. H., G. Brassard, C. Crépeau, R. Jozsa, A. Peres, and W. K. Wootters, *Phys. Rev. Lett.* **70**, 1895 (1993).
7. J. Chiaverini, D. Leibfried, T. Schaetz, M.D. Barrett, R.B. Blakestad, J. Britton, W.M. Itano, J.D. Jost, E. Knill, C. Langer, R. Ozeri & D.J. Wineland, *Nature* **432**, 602 (2004).
8. A. Rauschenbeutel, G. Nogues; S. Osnaghi, P. Bertet, M. Brune, J.-M. Raimond, S. Haroche, *Science* **288**, 2024 (2000).
9. C.A. Sackett, D. Kielpinski, B.E. King, C. Langer, V. Meyer, C.J. Myatt, M. Rowe, Q.A. Turchette, W.M. Itano, D.J. Wineland, and C. Monroe, *Nature* **404**, 256 (2000).
10. J. W. Pan, D. Bouwmeester, M.Daniell, H. Weinfurter, A. Zeilinger, *Nature* **403**, 515 (2000).
11. J. W. Pan, M. Daniell, S. Gasparoni, G. Weihs, A. Zeilinger, *Phys. Rev. Lett.* **86**, 4435 (2001).
12. M. Eibl, N. Kiesel, M. Bourennane, C. Kurtsiefer, H. Weinfurter, *Phys. Rev. Lett.* **92**, 077901 (2004).
13. Z. Zhao, Y.-A. Chen, A.-N. Zhang, T. Yang, H. Briegel, J.-W. Pan, *Nature* **430**, 54 (2004).
14. G. Teklemariam, E. M. Fortunato, M. A. Pravia, Y. Sharf, T. F. Havel, D. G. Cory, A. Bhattaharyya, and J. Hou , *Phys. Rev. A* **66**, 012309 (2002).
15. C. F. Roos, M. Riebe, H. Häffner, W. Hänsel, J. Benhelm, G. P. T. Lancaster, C. Becher, F. Schmidt-Kaler, R. Blatt, *Science* **304**, 1478 (2004).
16. R. Garisto and L. Hardy, *Phys. Rev. A* **60**, 827, (1999).
17. M. Riebe, H. Häffner, C. F. Roos, W. Hänsel, J. Benhelm, G. P. T. Lancaster, T. W. Körber, *Nature* **429**, 734 (2004).
18. F. Schmidt-Kaler, H. Häffner, M. Riebe, S. Gulde, G. P. T. Lancaster, T. Deuschle, C. Becher, C. F. Roos, J. Eschner & R. Blatt, *Nature* **422**, 408 (2003).
19. F. Schmidt-Kaler, H. Häffner, S. Gulde, M. Riebe, G. P.T. Lancaster, T. Deuschle, C. Becher, W. Hänsel, J. Eschner, C. F. Roos, R. Blatt, *Appl. Phys. B: Lasers and Optics* **77**, 789 (2003).
20. D. M. Greenberger, M. Horne, A. Zeilinger, in *Bell's Theorem, Quantum Theory, and Conceptions of the Universe*, edited by M. Kafatos (Kluwer Academic, Dordrecht, 1989).
21. W. Dür, G. Vidal, J. I. Cirac, *Phys. Rev. A* **62**, 062314 (2000).
22. A. Zeilinger, M. A. Horne D. M. Greenberger, NASA Conf. Publ. No. 3135 National Aeronautics and Space Administration, Code NTT, Washington, DC, (1997).
23. M. Šašura and V. Bužek, *J. Mod. Opt.* **49**, 1593 (2002).
24. D. F. V. James, P. G. Kwiat, W. J. Munro, A. G. White, *Phys. Rev. A* **64**, 052312 (2001).
25. D. Kielpinski, V. Meyer, M.A. Rowe, C.A. Sackett, W.M. Itano, C. Monroe, D.J. Wineland, *Science* **291**, 1013 (2001).
26. C. F. Roos, G. P. T. Lancaster, M. Riebe, H. Häffner, W. Hänsel, S. Gulde, C. Becher, J. Eschner, F. Schmidt-Kaler, R. Blatt, *Phys. Rev. Lett.* **92**, 220402

- (2004).
27. R. Raussendorf and H. J. Briegel, *Phys. Rev. Lett.* **86**, 5188 (2001).
 28. D. Gottesman D. & I.L. Chuang, *Nature* **402**, 390 (1999).
 29. D. Bouwmeester, J-W. Pan, K. Mattle, M. Eible, H. Weinfurter, and A. Zeilinger, *Nature* **390**, 575 (1997).
 30. D. Boschi, S. Branca, F. DeMartini, L. Hardy and S. Popescu, *Phys. Rev. Lett.* **80**, 1121 (1998).
 31. I. Marcikic, H. de Riedmatten, W. Tittel, H. Zbinden, & N. Gisin, *Nature* **421**, 509-513 (2003).
 32. D. Fattal, E. Diamanti, K. Inoue and Y. Yamamoto, *Phys. Rev. Lett.* **92**, 037904 (2004).
 33. A. Furusawa, J.L. Sørensen, S.L. Braunstein, C.A. Fuchs, H.J. Kimble, E.S. Polzik, *Science* **282**, 706 (1998).
 34. M. A. Nielsen, E. Knill & R. Laflamme, *Nature* **396**, 52 (1998).
 35. M. D. Barrett, J. Chiaverini, T. Schaetz, J. Britton, W.M. Itano, J.D. Jost, E. Knill, C. Langer, D. Leibfried, R. Ozeri & D.J. Wineland, *Nature* **429**, 737 (2004).
 36. D. Leibfried, B. DeMarco, V. Meyer, D. Lucas, M. Barrett, J. Britton, W. M. Itano, B. Jelenković, C. Langer, T. Rosenband & D. J. Wineland, *Nature* **422**, 412 (2003).
 37. J.I. Cirac and P. Zoller, *Phys. Rev. Lett.* **74**, 4091 (1995)
 38. K. Vogel and H. Risken, *Phys. Rev. A* **40**, 2847 (1989).
 39. S. Gulde, M. Riebe, G.P.T. Lancaster, C. Becher, J. Eschner, H. Häffner, F. Schmidt-Kaler, I.L. Chuang & R. Blatt, *Nature* **421**, 48 (2003).
 40. Steven van Enk, private communication.
 41. S. Massar and S. Popescu, *Phys. Rev. Lett.* **74**, 1259 (1995).
 42. N. Gisin, *Physics Letters A* **210**, 157 (1996).
 43. E.L. Hahn, *Phys. Rev.* **77**, 746 (1950)
 44. H. Häffner, S. Gulde, M. Riebe, G. Lancaster, C. Becher, J. Eschner, F. Schmidt-Kaler, and R. Blatt, *Phys. Rev. Lett.* **90**, 143602-1-4 (2003).